

A 3D Positioning-based Channel Estimation Method for RIS-aided mmWave Communications

Yaoshen Cui, Haifan Yin, Li Tan, and Marco Di Renzo, *Fellow, IEEE*

Abstract—A fundamental challenge in millimeter-wave (mmWave) communication is the susceptibility to blocking objects. One way to alleviate this problem is the use of reconfigurable intelligent surfaces (RIS). Nevertheless, due to the large number of passive reflecting elements on RIS, channel estimation turns out to be a challenging task. In this paper, we address the channel estimation for RIS-aided mmWave communication systems based on a localization method. The proposed idea consists of exploiting the sparsity of the mmWave channel and the topology of the RIS. In particular, we first propose the concept of reflecting unit set (RUS) to improve the flexibility of RIS. We then propose a novel coplanar maximum likelihood-based (CML) 3D positioning method based on the RUS, and derive the Cramer-Rao lower bound (CRLB) for the positioning method. Furthermore, we develop an efficient positioning-based channel estimation scheme with low computational complexity. Compared to state-of-the-art methods, our proposed method requires less time-frequency resources in channel acquisition as the complexity is independent to the total size of the RIS but depends on the size of the RUSs, which is only a small portion of the RIS. Large performance gains are confirmed in simulations, which proves the effectiveness of the proposed method.

Index Terms—Reconfigurable intelligent surface, intelligent reflecting surface, millimeter-wave communication, blockage, coverage, 3D-localization

I. INTRODUCTION

The commercialization of the fifth-generation (5G) of communications is in full swing and is facilitated by key technologies, such as massive multiple-input multiple-output (MIMO) systems and millimeter-wave (mmWave) communications. These technologies can significantly increase the network capacity and alleviate the spectrum shortage in wireless communication networks. However, mmWave communication systems are much more sensitive to blockages compared with microwave systems [2], which may undermine the potential of mmWave communications in some network deployments. The coverage problem at mmWave frequencies calls for solutions to make full use of the large available bandwidth.

A possible solution to counteract the coverage problem of mmWave systems is the deployment of reconfigurable intelligent surfaces (RIS) [3]–[5](also known as intelligent reflecting

This work was supported by the National Natural Science Foundation of China under grant No. 62071191. The corresponding author is Li Tan.

Yaoshen Cui, Haifan Yin, and Li Tan are with the School of Electronic Information and Communications, Huazhong University of Science and Technology, Wuhan, 430074, China (email: yaoshen_cui@hust.edu.cn; yin@hust.edu.cn; ltan@hust.edu.cn).

M. Di Renzo is with Université Paris-Saclay, CNRS, CentraleSupélec, Laboratoire des Signaux et Systèmes, 3 Rue Joliot-Curie, 91192 Gif-sur-Yvette, France. (marco.di-renzo@universite-paris-saclay.fr)

A part of this work [1] was presented in the 10th IEEE/CIC International Conference on Communications in China (IEEE/CIC ICCC 2021).

surfaces (IRSs) [6] and metasurfaces [7]). RIS is an emerging technology with the capability of intelligently manipulating the electromagnetic waves, which has lately drawn significant attentions as it has the potential of controlling the wireless propagation environment at a low hardware cost and energy consumption. The authors of [8], [9] developed free-space path loss models for RIS-aided systems based on the electromagnetic characteristics of RIS and validated them through simulations. In [10], the authors developed a new type of high-gain yet low-cost RIS with 256 elements, which operates at 2.3 GHz and 28.5 GHz. The authors of [11] demonstrated a prototype of RIS-aided communication system and showed some indoor and outdoor field trials with a fabricated RIS endowed with 1100 reflecting elements. The authors of [12] conceived a system for serving paired power-domain non-orthogonal multiple access (NOMA) users by designing the passive beamforming weights at the RIS.

In principle, the full potential of RIS can be achieved when the channel state information (CSI) is known. However, the RIS is usually not equipped with power amplifiers, digital signal processing units, multiple radio frequency chains and the number of reflecting elements is usually large, which make the CSI acquisition a challenging problem.

Recently, several strategies have been proposed to solve the problem of channel estimation in an RIS-aided system [13]. These include the cascaded channel decomposition approach [14]–[17], and methods based on the sparsity of channels [18]–[20], the quasi-static property [21], [22], etc. In a multiple-input single-output (MISO) system, the authors of [14], [15] decomposed the cascaded channel into a series of sub-channels, each of them corresponding to an RIS element, which are easier to be estimated. In a multi-user system, the authors of [16] proposed a three-phase pilot-based channel estimation protocol by activating users one by one. The authors of [17] developed two iterative estimation algorithms based on the parallel factor (PARAFAC) decomposition method. By exploiting the sparsity of the channels in the angular domain, the authors of [18], [19] formulated the cascaded channel estimation problem as a sparse signal recovery problem, which is solved by using compressive sensing (CS) algorithms. The authors of [20] proposed a two-stage algorithm for channel estimation by exploiting the bilinear sparse matrix factorization method. Since the base station (BS) and the RIS are usually deployed at fixed locations, the RIS-BS channel varies slowly and can be considered as quasi-static. The authors of [21], [22] developed a matrix-calibration-based method and a two-timescale channel estimation framework, respectively. These methods require less training overhead by exploiting the quasi-static property of the RIS-BS channel. However, these methods

generally require large training resources or high computation complexity, especially when the RIS is physically very large.

RIS has several applications for positioning as well [23]. In [24], the authors studied the possibility of RIS-aided localization and derived the corresponding Fisher information matrix (FIM) and the CRLB in closed-form expressions. The authors of [25] utilized an RIS to facilitate the positioning in conjunction with an ultra-wideband (UWB) indoor systems. The authors of [26] considered an RIS-aided mmWave MIMO system where the direct line of sight (LOS) is obstructed, and proposed an adaptive phase shift design based on hierarchical codebooks and feedback from the mobile station to enable joint localization and communication. Furthermore, conventional localization methods, such as those based on the received signal strength (RSS), the time of arrival (TOA), the time difference of arrival (TDOA) and the angle of arrival (AOA), can also be utilized for improving the localization performance in mmWave and massive MIMO systems [27].

In this paper, we propose an efficient channel estimation scheme that is based on a novel localization method. The method is designed for application to RIS-aided mmWave communication systems, and it exploits 1) the geometry of the RIS, 2) structural information of the wideband wireless channels, and 3) a new low-complexity coplanar maximum likelihood-based 3D positioning method. The main contributions of this paper are summarized as follows:

- We introduce the concept of *Reflecting Unit Set* (RUS), which is a set of neighboring reflecting units in a specific part of the RIS. A joint minimum mean square estimator (JMMSE) is proposed to calculate the distances between the RUSs and the user equipment (UE) based on the low-rank property of the wideband channel covariance matrix in the frequency domain. We utilize the RUSs as anchors to calculate the 3D location of the UE by exploiting the spatial structure of the wideband channel.
- We propose a coplanar maximum likelihood-based (CML) three-dimensional (3D) localization method that offers a high accuracy. Since the reflecting units of the RIS are coplanar, determining the 3D position of a target is a challenging problem. Closed-form expressions are derived for the localization of the target with the help of the RUSs based on the maximum likelihood (ML) criterion and the principles of Euclidean geometry.
- We derive a closed-form expression of the CRLB for the proposed scheme. We also show that its complexity does not depend on the number of reflecting units on the RIS, but it depends only on the number and size of the RUSs. As the size of RIS increases, the complexity of our proposed scheme remains low.

With the aid of numerical results, we show that the proposed method requires much lower computational complexity and uses much fewer time-frequency resources for channel acquisition compared with state-of-the-art methods [14]–[22]. The complexity and the pilot overhead of state-of-the-art methods depend on the total size of the RIS, which grows rapidly when increasing the size of the RIS. In contrast, the required complexity and the time-frequency resources of the proposed

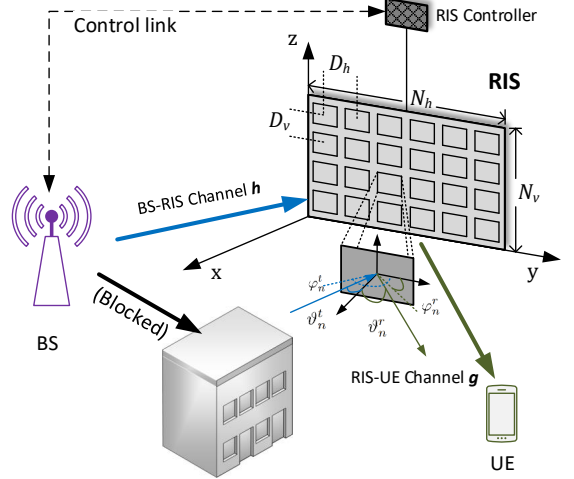


Fig. 1. RIS-assisted wireless communication system

method are just related to the size of a small portion of the RIS. Specially, we show that the proposed method needs around 20 orthogonal frequency division multiplexing (OFDM) symbols for channel estimation (or 0.167 ms with 120 kHz of subcarrier spacing in mmWave systems) [28], even in the presence of thousands reflecting units. To the best of our knowledge, this is the first low-cost CSI acquisition method for RIS-aided systems based on the RUS concept.

The remainder of this paper is organized as follows. In Section II, we describe the considered RIS-aided mmWave system and channel model. In Section III, we propose the channel estimation method based on 3D localization. In Section IV, we present numerical results for the proposed method. Finally, Section V concludes the paper.

Notation: We use bold-face symbols to denote vectors and matrices. $\mathbb{C}^{x \times y}$ denotes the space of $x \times y$ complex-valued matrices. \odot , $\lfloor \cdot \rfloor$ and \bmod stand for the Hadamard product, the rounding down and the remainder operation, respectively. For the vector \mathbf{x} , $\|\mathbf{x}\|$ denotes its the Euclidean norm and $\text{diag}(\mathbf{x})$ denotes a diagonal matrix with each diagonal element being the corresponding element in \mathbf{x} . \mathbf{X}^T , \mathbf{X}^* , \mathbf{X}^H and $\text{tr}(\mathbf{X})$ are the transpose, conjugate, conjugate transpose and trace of a matrix \mathbf{X} , respectively. \mathbf{I} denotes the identity matrix.

II. RIS-AIDED WIRELESS COMMUNICATIONS AND CHANNEL MODELING

We consider an RIS-aided mmWave communication system where the direct path between the BS and the UE is blocked by obstacles, as shown in Fig. 1. In this case, due to the high transmission frequency, the diffraction effects are negligible and the number of scattering paths is much smaller than in lower frequency bands (e.g., sub-6 GHz). The RIS is composed of N reflecting units and is deployed in the y - z plane of a Cartesian coordinate system. The bottom left corner of the RIS coincides with the origin of the coordinate system. The RIS is modeled as a uniform planar array (UPA) with N_h columns and N_v rows, and the area of each reflecting

element is $A_u = D_h \times D_v$, where D_h and D_v represent the element spacing along the horizontal and vertical directions, respectively. The gain and the normalized power radiation pattern¹ of each reflecting unit are denoted by G_u and $F(\vartheta, \varphi)$, where ϑ and φ are the zenith and azimuth angles, respectively.

We use $F_n^t = F(\vartheta_n^t, \varphi_n^t)$ and $F_n^r = F(\vartheta_n^r, \varphi_n^r)$ to represent the normalized power radiation pattern from the n -th reflecting unit of the RIS to the BS and from the n -th reflecting unit of the RIS to the UE, respectively, with $\vartheta_n^t, \varphi_n^t, \vartheta_n^r$ and φ_n^r representing the corresponding zenith and azimuth angles.

We introduce the vectors $\phi = [\phi_1, \dots, \phi_N]$ and $\beta = [\beta_1, \dots, \beta_N]$, where $\phi_n \in [0, 2\pi)$ and $\beta_n \in [0, 1]$, ($n = 1, \dots, N$) denote the phase shift and the amplitude of the reflection coefficient of the n -th reflecting unit of the RIS, respectively. The vector of reflection coefficients of the RIS, which is denoted by $\theta \in \mathbb{C}^{N \times 1}$, is expressed as

$$\begin{aligned} \theta &= [\theta_1, \dots, \theta_N]^T \\ &= [\beta_1 e^{j\phi_1}, \dots, \beta_N e^{j\phi_N}]^T, \end{aligned} \quad (1)$$

where $\theta_n = \beta_n e^{j\phi_n}$ ($n = 1, \dots, N$) denotes the reflection coefficient of the n -th reflection unit of the RIS.

In the considered RIS-aided mmWave system, we mainly consider the LOS links between the transceivers and the RIS, which are usually much stronger than other multipath components in the mmWave band [29], [30]. Without loss of generality, we consider a single-input single-output (SISO) setting, yet the proposed method can be readily generalized to a multiple-antenna BS/UE setting. The channel between the BS and the n -th reflecting unit is denoted by h_n and can be expressed as [8]

$$h_n = \sqrt{\frac{A_u F_n^{tx} F_n^t}{4\pi d_{t,n}^2}} e^{-\frac{j2\pi d_{t,n}}{\lambda}}, \quad (2)$$

where λ denotes the wavelength, $F_n^{tx} = F^{tx}(\vartheta_n^{tx}, \varphi_n^{tx})$ denotes the normalized power radiation pattern of the transmit antenna from the BS to the n -th reflecting unit of the RIS with ϑ_n^{tx} and φ_n^{tx} denoting the corresponding zenith and azimuth angles, and $d_{t,n}$ denotes the distance between the BS and the n -th reflecting unit of the RIS.

Based on (2), the LOS channel vector between the BS and the RIS, which is denoted by $\mathbf{h} \in \mathbb{C}^{N \times 1}$, is expressed as

$$\begin{aligned} \mathbf{h} &= [h_1, \dots, h_N]^T \\ &= \left[\sqrt{\frac{A_u F_1^{tx} F_1^t}{4\pi d_{t,1}^2}} e^{-\frac{j2\pi d_{t,1}}{\lambda}}, \dots, \sqrt{\frac{A_u F_N^{tx} F_N^t}{4\pi d_{t,N}^2}} e^{-\frac{j2\pi d_{t,N}}{\lambda}} \right]^T. \end{aligned} \quad (3)$$

Similarly, the LOS channel between the UE and the n -th reflecting unit is denoted by g_n and is expressed as

$$g_n = \sqrt{\frac{A_r F_n^{rx} F_n^r}{4\pi d_{r,n}^2}} e^{-\frac{j2\pi d_{r,n}}{\lambda}}, \quad (4)$$

where A_r denotes the aperture of the receive antenna, $F_n^{rx} = F^{rx}(\vartheta_n^{rx}, \varphi_n^{rx})$ denotes the normalized power radiation pattern of the receive antenna from the UE to the n -th reflecting unit

¹The power radiation pattern quantifies the amount of power radiated or received by an antenna as a function of the direction of observation with respect to the center of the antenna.

of the RIS with ϑ_n^{rx} and φ_n^{rx} denoting the zenith and azimuth angles, and $d_{r,n}$ is the distance between the receiver UE and the n -th reflecting unit of the RIS.

Based on (4), the LOS channel between the UE and the RIS, which is denoted by $\mathbf{g} \in \mathbb{C}^{N \times 1}$, is expressed as:

$$\begin{aligned} \mathbf{g} &= [g_1, \dots, g_N]^T \\ &= \left[\sqrt{\frac{A_r F_1^{rx} F_1^r}{4\pi d_{r,1}^2}} e^{-\frac{j2\pi d_{r,1}}{\lambda}}, \dots, \sqrt{\frac{A_r F_N^{rx} F_N^r}{4\pi d_{r,N}^2}} e^{-\frac{j2\pi d_{r,N}}{\lambda}} \right]^T. \end{aligned} \quad (5)$$

Given the BS-RIS channel and the RIS-UE channel in (3) and (5), the cascaded BS-RIS-UE channels can be expressed as:

$$\begin{aligned} w &= \left((\sqrt{G_r} \mathbf{g}) \odot (\sqrt{G_t} \mathbf{h}) \right)^T (\sqrt{G_u} \boldsymbol{\theta}) \\ &= \sqrt{G_r G_u G_t} (\mathbf{g} \odot \mathbf{h})^T \boldsymbol{\theta} \\ &= \frac{\sqrt{G_r G_u G_t A_r A_u}}{4\pi} \sum_{n=1}^N \frac{\sqrt{\tilde{F}_n} \theta_n}{d_{t,n} d_{r,n}} e^{-\frac{j2\pi(d_{t,n} + d_{r,n})}{\lambda}} \end{aligned} \quad (6)$$

where G_t denotes the transmit antenna gain, G_r denotes the receive antenna gain and $\tilde{F}_n = F_n^{tx} F_n^t F_n^{rx} F_n^r$ accounts for the effect of the normalized power radiation patterns on the received signal power.

When the BS transmits the signal s to the RIS, the signal received by the UE is

$$r = sw + \eta = s \frac{\sqrt{G_r G_u G_t A_r A_u}}{4\pi} \sum_{n=1}^N \frac{\sqrt{\tilde{F}_n} \theta_n}{d_{t,n} d_{r,n}} e^{-\frac{j2\pi(d_{t,n} + d_{r,n})}{\lambda}} + \eta \quad (7)$$

where $\eta \sim \mathcal{CN}(0, \sigma^2)$ denotes the additive white Gaussian noise (AWGN) at the UE whose variance is σ^2 .

We aim to maximize the received power P_r at the UE side by optimizing the reflection coefficient vector $\boldsymbol{\theta}$ based on the available CSI. The problem can be formulated as

$$\check{\boldsymbol{\theta}} = \underset{\boldsymbol{\theta}}{\operatorname{argmax}} \{ |(\mathbf{g} \odot \mathbf{h})^T \boldsymbol{\theta}|^2 \}. \quad (8)$$

Ideally, when the CSI is perfectly known, the optimal reflection coefficient of the n -th reflecting unit of the RIS can be expressed as

$$\check{\theta}_n = \frac{g_n^* h_n^*}{|g_n h_n|}, n = 1, \dots, N. \quad (9)$$

Nevertheless, the CSI has to be estimated beforehand. Due to the large number of RIS reflecting elements and the unavailability of signal processing units at the RIS, the CSI acquisition process is a challenging task. Moreover, the time-varying locations of the UE make it imperative to learn the channel within a very short time. In the next section, we will propose an efficient method for channel estimation to address these issues.

III. PROPOSED CSI ACQUISITION SCHEME BASED ON 3D LOCALIZATION

In this section, we show the localization-based channel estimation method. The proposed approach capitalizes on two properties of mmWave channels: 1) The sparsity and the structural information of the mmWave channel that is dominated by

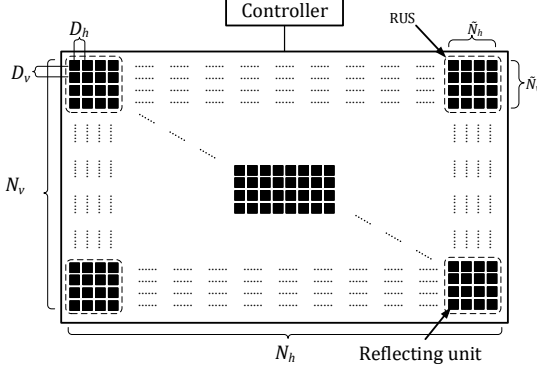


Fig. 2. The model of RIS with RUSs

the LOS path; 2) The different distances between the reflecting units and the UE. Since the positions of the RIS and the BS are generally fixed, the BS-RIS channel is quasi-static and is assumed known. Our target is to estimate the RIS-UE channel by performing a two-step 3D localization scheme, which is based on a concept named reflecting unit set (RUS), as shown in Fig. 2. These RUSs are utilized as *anchor nodes* to locate the position of the UE. More details are given below.

A. Reflecting Unit Set

RUS is a set of reflecting units in a specific part of the RIS, which can beamform the incident signal to the UE, provided that a proper set of phase shifts is applied to the elements of the RUS. For ease of exposition, we assume all M RUSs have the same shape and size: a rectangular structure with $\tilde{N} = \tilde{N}_h \times \tilde{N}_v$ reflecting units, where \tilde{N}_h and \tilde{N}_v represent the numbers of columns and rows of the reflecting elements within one RUS, respectively.

The key characteristics of an RUS are as follows:

1) *Active State*: An RUS is in the *active* state when the reflecting elements inside the RUS reflect the incident signals. If the state is *inactive*, on the other hand, the elements do not reflect the signal of interest, i.e., the electromagnetic waves are absorbed. Examples of metamaterials with these property are given in [31], [32]. In addition, the elements of the RUS may be equipped with amplifiers in order to enhance the reflected signal [33].

2) *Codebook and Codeword*: The codebook of an RUS is a set of codewords, which are used as the vectors of reflection coefficients of the RUS to beamform the incident radio waves to different directions. Since the RUS is selected as an UPA, we may adopt the discrete Fourier transform (DFT) based codebook as defined in [34]

$$\mathbf{u}_p = \left[1 \quad e^{j \frac{2\pi p}{O_1 \tilde{N}_v}} \quad \dots \quad e^{j \frac{2\pi p(\tilde{N}_v-1)}{O_1 \tilde{N}_v}} \right], \quad (10)$$

$$\mathbf{v}_{l,p} = \left[\mathbf{u}_p \quad e^{j \frac{2\pi l}{O_2 \tilde{N}_h}} \mathbf{u}_p \quad \dots \quad e^{j \frac{2\pi l(\tilde{N}_h-1)}{O_2 \tilde{N}_h}} \mathbf{u}_p \right]^T. \quad (11)$$

The codewords are $\mathbf{v}_{l,p} \in \mathbb{C}^{\tilde{N}_h \tilde{N}_v \times 1}$ with $p = 1, \dots, \tilde{N}_v$ and $l = 1, \dots, \tilde{N}_h$ being the indices of the vertical and horizontal beam directions, respectively. O_1 and O_2 are the vertical and horizontal oversampling factors that may take positive integer

values. We set the order of the reflecting units of the RUS as follows: starting from the lower left corner of the RUS, the number increases along the first column, then the second, etc, until the \tilde{N}_h -th column. The relationship between the indices of the vertical and horizontal beam directions and the index of the codeword (denoted by $\tilde{n} \in [1, \tilde{N}]$) can be expressed as:

$$\tilde{n} = (l-1)\tilde{N}_v + p, \quad (12)$$

and then the \tilde{n} -th codeword can be defined as $\tilde{\theta}_{\tilde{n}} \triangleq \mathbf{v}_{l,p}$. The corresponding codebook, denoted by $\tilde{\Theta}$, can be expressed as

$$\tilde{\Theta} = [\tilde{\theta}_1, \dots, \tilde{\theta}_{\tilde{N}}]. \quad (13)$$

3) *Selection of Codeword*: The RUS can be seen as a small RIS. According to (6), the cascaded BS-RUS-UE channel corresponding to the \tilde{n} -th codeword is expressed as

$$\tilde{w}_{\tilde{n}} = \sqrt{G_r G_u G_t} (\tilde{\mathbf{g}} \odot \tilde{\mathbf{h}})^T \tilde{\theta}_{\tilde{n}}, \quad (14)$$

where $\tilde{\mathbf{h}}$ and $\tilde{\mathbf{g}}$, derived from (2)-(3) and (4)-(5) respectively, denote the BS-RUS channel and the RUS-UE channel. Based on (7), the received signal at the UE via the RUS is

$$\tilde{r}_{\tilde{n}} = s \tilde{w}_{\tilde{n}} + \eta. \quad (15)$$

We then choose from the codebook a codeword that maximizes the received signal strength at the UE, and the index of the selected codeword can be expressed as

$$\tilde{n}_{opt} = \underset{\tilde{n}}{\operatorname{argmax}} \{ \tilde{r}_{\tilde{n}} \}. \quad (16)$$

It may take several trials to find an optimal codeword. An ordinary strategy is traversing all codewords in the codebook $\tilde{\Theta}$ to select the codeword. The same selected codeword can be used in a certain time interval, and even re-used by all the RUSs. This will help reduce the complexity at the cost of a weaker pilot signal reception at the UE.

Note that the shape of the RUS is not limited to a UPA, and the size of the RUS can be customized. Smaller RUS may provide better accuracy when the reflected signal is strong enough for the UE to acquire good channel estimation quality. However, when the strength of the desired reflective radio wave is not guaranteed, the size of the RUS should be larger, or the RUSs should be equipped with power amplifiers.

We then estimate the RUS-UE distances based on the angle-delay structure of the wideband mmWave channels.

B. RUS-UE Distance Estimations

Due to the limited multipath delay distribution, the channel covariance matrix in the frequency domain has a low rank, which can be exploited to enhance the delay estimation performance. With ultra-wide bandwidth, mmWave communications can offer higher resolution of the delay and improve the accuracy of the distance estimation. In this section, we propose a distance estimation method exploiting the low rank of the frequency-domain channel covariance matrix.

The whole bandwidth F_d with central frequency F_c is equally divided into K sub-bands, where the k -th sub-band has a center frequency of f_k and a corresponding wavelength $\lambda_k = \frac{c}{f_k}$ (c denotes the speed of light). The vector of

frequencies is denoted as $\mathbf{f} = [f_1, \dots, f_K]$. Denoting the noise power spectral density as $\bar{\sigma}^2$, the noise power at each sub-band is $\sigma_n^2 = \bar{\sigma}^2 f_d$, where f_d is the bandwidth of each sub-band. Without loss of generality, the total transmit power P_t is equally allocated to K sub-bands and the transmit power of a sub-band is $\sigma_t^2 = P_t/K$.

The received signal at the k -th sub-band via the m -th RUS (denoted as RUS_m) is expressed by

$$\tilde{r}_{m,k} = s_{m,k} \tilde{w}_{m,k} + \eta_{m,k}, \quad (17)$$

where $\tilde{s}_{m,k}$, $\tilde{w}_{m,k}$ and $\eta_{m,k} \sim \mathcal{CN}(0, \sigma_n^2)$ denote the transmitted signal, the cascaded channel via RUS_m at k -th sub-band and the AWGN at the UE, respectively. We show more details of several distance estimation methods below.

1) *Matrix Pencil (MP)-based Method*: According to the low-rank property and the wideband setting, we develop a Matrix Pencil [35] based distance estimation method. Considering the cascaded channel via the m -th RUS with \tilde{N} units and the proper codeword, the relationship between the wavelength of the K sub-bands can be expressed as

$$\lambda_k = \frac{c}{f_1 + (k-1)f_d}, \quad k = 1, \dots, K. \quad (18)$$

Then based on the one-dimensional MP method [36], the estimated distance between the UE and the m -th RUS can be expressed as

$$\hat{d}_m = \frac{1}{\tilde{N}} \sum_{\tilde{n}=1}^{\tilde{N}} \frac{c \log \tilde{z}_{\tilde{n}}}{-j2\pi f_d} - d_{bs,m} \quad (19)$$

where

$$\tilde{z}_{\tilde{n}} = e^{\frac{-j2\pi(d_{t,\tilde{n}} + d_{r,\tilde{n}})f_d}{c}}, \quad \tilde{n} = 1, \dots, \tilde{N}, \quad (20)$$

denotes the eigenvalue of the Hankel matrix product for matrix pencil method and $d_{bs,m}$ denotes the BS-RUS $_m$ distance.

2) *Conventional MMSE-based Method*: Adopting the conventional MMSE-based estimation criterion, we show the MMSE channel estimation independently for each sub-band, when the RUS_m is activated and a proper codeword is chosen.

Based on (17), with the MMSE method, the estimated cascaded channel of the k -th sub-band via the m -th RUS is expressed as

$$\hat{w}_{m,k} = R_{m,k} s_{m,k}^* (\sigma_t^2 R_{m,k} + \sigma_n^2)^{-1} \tilde{r}_{m,k}, \quad (21)$$

where $R_{m,k} = \mathbb{E}[\tilde{w}_{m,k} \tilde{w}_{m,k}^*]$ denotes the covariance coefficient of the cascaded channel of the k -th sub-band and the m -th RUS. The mean squared error (MSE) of the estimation is

$$\begin{aligned} \mathcal{M}_{m,k} &= \mathbb{E}\{\|\hat{w}_{m,k} - \tilde{w}_{m,k}\|^2\} \\ &= R_{m,k} \left(1 + \frac{\sigma_t^2}{\sigma_n^2} R_{m,k}\right)^{-1}, \\ &= \frac{R_{m,k} \sigma_n^2}{\sigma_t^2 R_{m,k} + \sigma_n^2} \end{aligned} \quad (22)$$

Based on (21), the estimated cascaded channel vector of the m -th RUS is expressed as

$$\hat{\mathbf{w}}_m = [\hat{w}_{m,1}, \hat{w}_{m,2}, \dots, \hat{w}_{m,K}]^T. \quad (23)$$

and the distance between the UE and the RUS_m can be acquired by Bartlett's method [37].

3) *Proposed Joint MMSE (JMMSE)-based Method*: In order to give full play to the role of ultra-wideband, we develop a JMMSE-based distance estimation method which is able to exploit the low-rankness structure of the covariance matrix in the frequency domain [38]. When the RUS_m is activated and a proper codeword is chosen, we estimate the corresponding RUS-UE distance with the JMMSE channel estimation of all sub-bands.

The BS-RUS $_m$ -UE channel with K sub-bands is expressed as

$$\tilde{\mathbf{w}}_m = [\tilde{w}_{m,1}, \tilde{w}_{m,2}, \dots, \tilde{w}_{m,K}]^T, \quad (24)$$

where $\tilde{w}_{m,k}$ ($k = 1, \dots, K$) is the cascaded BS-RUS $_m$ -UE channel at the k -th sub-band.

The received signal of all K sub-bands via RUS_m is expressed as

$$\tilde{\mathbf{r}}_m = \mathbf{S}_m \tilde{\mathbf{w}}_m + \boldsymbol{\eta}_m, \quad (25)$$

where $\tilde{\mathbf{r}}_m = [\tilde{r}_{m,1}, \dots, \tilde{r}_{m,K}]^T$, $\boldsymbol{\eta}_m = [\eta_{m,1}, \dots, \eta_{m,K}]^T$ and $\mathbf{S}_m = \text{diag}([s_{m,1}, \dots, s_{m,K}]^T)$ denote the received signal vector, the noise vector and the transmitted signal vector of all K sub-bands via the m -th RUS.

With the JMMSE estimation method, the estimated cascaded channel via RUS_m is expressed as

$$\hat{\mathbf{w}}_m = \mathbf{R}_m (\mathbf{R}_m + \frac{\alpha \sigma_n^2}{\sigma_t^2} \mathbf{I})^{-1} \mathbf{S}_m^{-1} \tilde{\mathbf{r}}_m \quad (26)$$

where $\mathbf{R}_m = \mathbb{E}[\tilde{\mathbf{w}}_m \tilde{\mathbf{w}}_m^H]$ is the covariance matrix of the channel in the frequency domain and α is a parameter of regularization. With the true delay denoted by t_m , the estimated delay of the BS-RUS $_m$ -UE channel can be calculated as

$$\begin{aligned} \hat{t}_m &= \underset{t_m}{\text{argmax}} \{\|\hat{\mathbf{w}}_m^T \mathbf{b}(t_m)\|^2\} \\ &= t_m + \Delta t_m, \end{aligned} \quad (27)$$

where Δt_m denotes the error of the estimated delay and $\mathbf{b}(t) \in \mathbb{C}^{K \times 1}$ is defined as

$$\mathbf{b}(t) = [e^{j2\pi f_1 t}, \dots, e^{j2\pi f_K t}]^T. \quad (28)$$

The distance between the UE and RUS_m is $d_m = c(t_m - t_{bs,m})$, and the estimated one is expressed as

$$\begin{aligned} \hat{d}_m &= c(\hat{t}_m - t_{bs,m}) \\ &= d_m + \Delta d_m, \end{aligned} \quad (29)$$

where $\Delta d_m = c\Delta t_m$ denotes the estimated error of the distance of UE-RUS $_m$ channel, and $t_{bs,m}$ denotes the true delay of BS-RUS $_m$ channel. Since the BS and the RIS are generally fixed, their locations and the delay $t_{bs,m}$ can be assumed known.

C. Proposed Coplanar ML-based 3D Localization Method

Note that all the anchors (i.e., RUSs) are on the same plane (y-z plane), which makes most trilateration localization methods fail to work, such as those based on least squares matrix [39]. The authors of [40] and [41] gave alternate ML-based solutions for TDOA and TOA estimation in 2D settings where all anchors are collinear. In this paper, we develop a novel

coplanar maximum likelihood-based (CML) 3D localization method for the RIS-aided communication system.

The position of the UE is $\mathbf{p} = (x, y, z)$ and the vector of the measured distances between the UE and all M RUS is expressed as

$$\hat{\mathbf{d}} = [\hat{d}_1, \hat{d}_2, \dots, \hat{d}_M]^T = \mathbf{d} + \mathbf{e}, \quad (30)$$

where $\mathbf{d} = [d_1, d_2, \dots, d_M]^T$ and $\mathbf{e} = [e_1, \dots, e_M]^T$ denote the vectors of the corresponding actual distances and additive measurement errors, respectively.

Based on (25) and (26), the estimated error of the BS-RUS _{m} -UE channel is

$$\begin{aligned} \mathbf{e}_{wm} &= \hat{\mathbf{w}}_m - \mathbf{w}_m \\ &= (\mathbf{A} - \mathbf{I})\mathbf{w}_m + \mathbf{A}\mathbf{S}^{-1}\boldsymbol{\eta}_m \end{aligned} \quad (31)$$

where $\mathbf{A} = \mathbf{R}_m(\mathbf{R}_m + \frac{\alpha\sigma_n^2}{\sigma_d^2}\mathbf{I})^{-1}$. When the SNR is high, \mathbf{A} is close to \mathbf{I} , and then \mathbf{e}_{wm} follows a zero-mean Gaussian distribution. Based on this fact, each entry of \mathbf{e} is modeled as a Gaussian distribution with zero mean and variance σ_d^2 , i.e., $e_m \sim \mathcal{CN}(0, \sigma_d^2)$, $m = 1, \dots, M$, and the conditional probability density function (PDF) of the measured distance \hat{d} is expressed as

$$P(\hat{\mathbf{d}}|\mathbf{p}) = (2\pi\sigma_d^2)^{-\frac{M}{2}} \exp\left(-\frac{J}{2\sigma_d^2}\right), \quad (32)$$

where

$$J = \sum_{m=1}^M (d_m - \hat{d}_m)^2. \quad (33)$$

Based on the maximum likelihood criterion, the problem of finding \mathbf{p} from $\hat{\mathbf{d}}$ is to minimize (33).

For the given four specific coplanar RUSs, the coordinates are $\mathbf{p}_1 = (0, 0, 0)$, $\mathbf{p}_2 = (0, a, 0)$, $\mathbf{p}_3 = (0, a, b)$ and $\mathbf{p}_4 = (0, 0, b)$ (both a and b are real), and the measured distances between each anchor and the UE to be localized are \hat{d}_m ($m = 1, \dots, 4$), respectively. Then, the actual distances are defined by

$$d_1 = (x^2 + y^2 + z^2)^{\frac{1}{2}}, \quad (34)$$

$$d_2 = [x^2 + (y - a)^2 + z^2]^{\frac{1}{2}}, \quad (35)$$

$$d_3 = [x^2 + (y - a)^2 + (z - b)^2]^{\frac{1}{2}}, \quad (36)$$

$$d_4 = [x^2 + y^2 + (z - b)^2]^{\frac{1}{2}}. \quad (37)$$

The closed-form solutions for minimizing (33) are shown in Theorem 1.

Theorem 1 *The maximum likelihood (ML) estimation of the distances are*

$$d_1 = \frac{\hat{d}_1 \left(\hat{d}_1^2 + \hat{d}_3^2 \pm \sqrt{(\hat{d}_1^2 + \hat{d}_3^2)(\hat{d}_2^2 + \hat{d}_4^2)} \right)}{2(\hat{d}_1^2 + \hat{d}_3^2)}, \quad (38)$$

$$d_2 = \frac{\hat{d}_2 d_1}{2d_1 - \hat{d}_1}, \quad (39)$$

$$d_3 = \frac{\hat{d}_3 d_1}{\hat{d}_1}, \quad (40)$$

$$d_4 = \frac{\hat{d}_4 d_1}{2d_1 - \hat{d}_1}, \quad (41)$$

Proof: To minimize (33), we differentiate J with respect to x , y and z and set the results to zero

$$\frac{\partial J}{\partial x} = \sum_{m=1}^4 \frac{2x(d_m - \hat{d}_m)}{d_m} \quad (42)$$

$$\frac{\partial J}{\partial y} = \sum_{m=1}^4 \frac{2y(d_m - \hat{d}_m)}{d_m} - \sum_{m=2,3} \frac{2a(d_m - \hat{d}_m)}{d_m} \quad (43)$$

$$\frac{\partial J}{\partial z} = \sum_{m=1}^4 \frac{2z(d_m - \hat{d}_m)}{d_m} - \sum_{m=2,4} \frac{2b(d_m - \hat{d}_m)}{d_m} \quad (44)$$

Combining (42) - (44), d_2 , d_3 and d_4 can be formulated in terms of d_1

$$d_2 = \frac{\hat{d}_2 d_1}{2d_1 - \hat{d}_1}, \quad d_3 = \frac{\hat{d}_3 d_1}{\hat{d}_1}, \quad d_4 = \frac{\hat{d}_4 d_1}{2d_1 - \hat{d}_1} \quad (45)$$

From (34)-(37), the relationship among d_1 , d_2 , d_3 and d_4 can be expressed as

$$d_1^2 + d_3^2 - d_2^2 - d_4^2 = 0. \quad (46)$$

Then, substituting (45) into (46), we have

$$\frac{4K_{13}d_1^4}{\hat{d}_1^2} - \frac{4K_{13}d_1}{\hat{d}_1^3} + (K_{13} - K_{24})d_1^2 = 0 \quad (47)$$

where $K_{13} = \hat{d}_1^2 + \hat{d}_3^2 > 0$ and $K_{24} = \hat{d}_2^2 + \hat{d}_4^2 > 0$. Since $d_m > 0$, (47) can be solved by

$$\begin{aligned} d_1 &= \frac{\hat{d}_1(K_{13} \pm \sqrt{K_{13}K_{24}})}{2K_{13}} \\ &= \frac{\hat{d}_1 \left(\hat{d}_1^2 + \hat{d}_3^2 \pm \sqrt{(\hat{d}_1^2 + \hat{d}_3^2)(\hat{d}_2^2 + \hat{d}_4^2)} \right)}{2(\hat{d}_1^2 + \hat{d}_3^2)}. \end{aligned} \quad (48)$$

Finally, d_2 , d_3 , d_4 can be derived from (45) and (48). \square

Since at least one root of d_1 is positive, we choose the correct root as follows. If only one root is positive, it is the value we needed. If all roots are positive, the one that gives the smaller J in (33) is selected.

According to (34)-(37), Theorem 1, and Euclidean geometry, the 3D position $\mathbf{p} = (x, y, z)$ of the UE can be solved by

$$y = \frac{\bar{d}_1^2 - \bar{d}_2^2 - \bar{d}_3^2 + \bar{d}_4^2 + 2a^2}{4a}, \quad (49)$$

$$z = \frac{\bar{d}_1^2 + \bar{d}_2^2 - \bar{d}_3^2 - \bar{d}_4^2 + 2b^2}{4b}, \quad (50)$$

$$x = \sqrt{\bar{d}_m^2 - (y - \mathbf{p}_m(y))^2 - (z - \mathbf{p}_m(z))^2}, \quad (51)$$

where $m = 1, 2, 3, 4$ and we assume the UE and the BS are in the front side of the RIS, which means $\bar{x} > 0$ for the UE position, as shown in Fig. 1. The CML selects the $\mathbf{p} = (x, y, z)$ that gives the minimum J .

Furthermore, the constraints on the positions of the RUSs can be relaxed, i.e., they are not necessarily on the four corners of the RIS, and our method can be extended naturally if we transform the basis of the y-z plane based on the properties of the linear transformation space.

The closed-form Fisher Information Matrix and the Cramer-Rao lower bounds (CRLBs) for the 3D positioning based on the RUSs are shown in Theorem 2.

Theorem 2 *The elements of Fisher Information Matrix (FIM) denoted by Ψ is expressed as*

$$\begin{aligned} \Psi_{ij} &= -\mathbb{E}\left[\frac{\partial^2 \ln P(\hat{\mathbf{d}}|\mathbf{p})}{\partial \mathbf{p}(i) \partial \mathbf{p}(j)}\right] \\ &= \sum_{m=1}^M \frac{1}{\sigma_d^2} \frac{(\mathbf{p}(i) - \mathbf{p}_m(i))(\mathbf{p}(j) - \mathbf{p}_m(j))}{d_m^2}, \end{aligned} \quad (52)$$

where $i, j = 1, 2, 3$, and $\mathbf{p}_m = (x_m, y_m, z_m)$ denotes the location of the m -th anchor node.

Then, the CRLB matrix of the CML 3D localization method is

$$\mathbf{C} = \begin{bmatrix} C_{11} & C_{12} & C_{13} \\ C_{21} & C_{22} & C_{23} \\ C_{31} & C_{32} & C_{33} \end{bmatrix} = \Psi^{-1}, \quad (53)$$

where C_{11} , C_{22} and C_{33} denote the CRLBs of the estimation of the (x, y, z) coordinates respectively.

Proof: See Appendix A. \square

Overall, with the position of the UE estimated by our two-step localization scheme that includes the distance estimation phase and CML-based 3D localization phase, we may obtain the estimation of the channel \mathbf{g} and further compute the reflecting coefficient vector θ , according to Section II. Taking the JMMSE-based method as an example, we summarize the procedure in Algorithm 1.

Note that the radiation patterns are not necessary when computing the optimal reflection coefficients θ , only the path delay $d_{r,n} = \|\mathbf{p} - \mathbf{p}_n\|, n = 1, \dots, N$ is sufficient. The complexity order of our method is $\mathcal{O}(MN\tilde{N})$, which does not depend on the total number of reflecting units on the RIS. It helps to keep the complexity low, especially for a large RIS. As the size of the RIS increases, the complexity and training overhead of most prior works will increase significantly. For a large RIS, our proposed scheme has a better performance due to the exploitation of the differences of the RUS-UE

Algorithm 1 The Proposed JMMSE and CML based Channel Estimation Scheme

Input: $\mathbf{h}, \mathbf{S}, \mathbf{p}_{bs}, \mathbf{p}_m, m = 1, \dots, M, \mathbf{p}_n, n = 1, \dots, N$

- 1: **for** $m = 1, \dots, M$ **do**
- 2: Activate the m -th RUS to reflect the transmitted signal;
- 3: % Choose the optimal codeword of the m -th RUS.
- 4: **for** $\tilde{n} = 1, \dots, N$ **do**
- 5: Select the \tilde{n} -th codeword $\tilde{\theta}_{\tilde{n}}$ for the RUS;
- 6: UE receives the wideband pilot signal:
- 7: $\tilde{\mathbf{r}}_{\tilde{n}} = [\tilde{r}_{\tilde{n},1}, \dots, \tilde{r}_{\tilde{n},K}]^T$
- 8: **end for**
- 9: $\tilde{n}_{opt} = \operatorname{argmax}_{\tilde{n}}(\|\tilde{\mathbf{r}}_{\tilde{n}}\|)$;
- 10: Estimate the BS-RUS $_m$ -UE wideband channel based on JMMSE (26);
- 11: Estimate the channel delay based on (27) and (28);
- 12: **end for**
- 13: % Localization of the UE with the CML method.
- 14: Determine the position of the UE \mathbf{p} based on Theorem 1 and (49)-(51);
- 15: % Channel reconstruction.
- 16: Calculate the distance between the UE and the elements of the RIS: $d_{r,n} = \|\mathbf{p} - \mathbf{p}_n\|, n = 1, \dots, N$;
- 17: Reconstruct the RIS-UE channel \mathbf{g} based on (5);

Output: \mathbf{p}, \mathbf{g}

distances. In practice, the number of RUSs can be set to $M = 4$ according to the CML method, and the number of reflecting units on each RUS is much smaller than that on the overall RIS ($\tilde{N} \ll N$).

Consider for example an RIS with four RUSs, each of the RUS has four rows and four columns of reflecting units. A DFT codebook containing 16 codewords is used. Assuming the same codeword is shared by all RUSs, the searching of the codeword takes 16 OFDM symbols. Four more symbols are needed to complete activating all RUSs. Thus the total number of OFDM symbols needed can be limited to 20. In general, the above proposed method can be completed efficiently with low time-frequency resource utilization.

IV. NUMERICAL RESULTS

In this section, we verify the feasibility of the proposed method through multiple simulations and analyze its performance and robustness. We consider an RIS-aided mmWave communication in a 3D coordinate system as shown in Fig. 1. The coordinates of the BS are $(5, -5, 2)$ (meters), and the LOS path between the BS and the UE is assumed to be negligible due to the presence of blocking objects. The main simulation parameters are shown in Table I. The RIS, located in the y-z plane with the center located at $\mathbf{p}_c = (0, 0.32, 0.16)$, contains $N = N_v \times N_h$ reflecting units. We set $M = 4$ RUSs at the four corners of RIS whose size $\tilde{N} = \tilde{N}_h \times \tilde{N}_v$ as shown in Fig. 2. The total transmit power is $P_t = 30$ dBm, the gain of each reflecting unit is $G_u = 9.03$ dBi [8], the antenna gains of the transmit antenna and receive antenna are $G_t = G_r = 21$ dBi, the aperture of the receive antenna $A_r = \frac{\lambda^2}{4\pi}$, and the normalized power radiation patterns of the transmit and receive

TABLE I
SIMULATION PARAMETERS

| Symbol | Value | Definition |
|---------------------------|--------|--|
| N | 8192 | Number of reflecting units on the RIS |
| N_v | 64 | Number of rows of reflecting units on the RIS |
| N_h | 128 | Number of columns of reflecting units on the RIS |
| $D_v(\text{m})$ | 0.005 | Row spacing between adjacent units |
| $D_h(\text{m})$ | 0.005 | Column spacing between adjacent units |
| M | 4 | Number of RUSs on the RIS |
| \tilde{N} | 16 | Number of reflecting units on an RUS |
| \tilde{N}_v | 4 | Number of rows of reflecting units on an RUS |
| \tilde{N}_h | 4 | Number of columns of reflecting units on an RUS |
| $F_c(\text{GHz})$ | 28 | Center frequency |
| $F_d(\text{Mhz})$ | 3.6 | Bandwidth of a subband (5 resource blocks) |
| K | 128 | Number of subbands |
| $\sigma^2(\text{dBm/Hz})$ | -170 | Noise power spectral density |
| α | 10^4 | Coefficient of regularization |

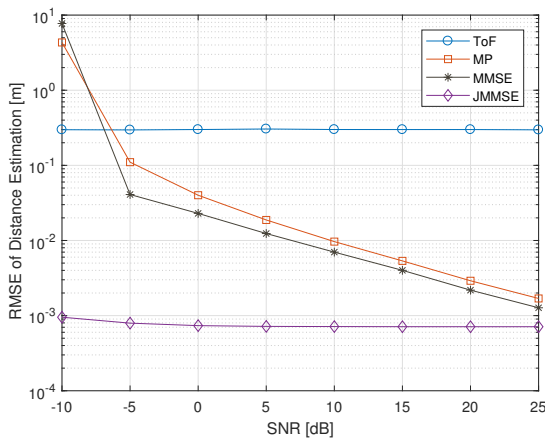


Fig. 3. The RMSE performance of distance estimation vs SNR of the received signal via the RUSs.

antennas are $F_n^{tx} = F_n^{rx} = 1$, $n = 1, \dots, N$. The normalized power radiation pattern of each reflecting unit is:

$$F(\vartheta, \varphi) = \begin{cases} \cos^3(\vartheta) & \vartheta \in [0, \frac{\pi}{2}], \varphi \in [0, 2\pi] \\ 0 & \vartheta \in (0, \frac{\pi}{2}], \varphi \in [0, 2\pi] \end{cases} \quad (54)$$

For a fixed UE with coordinate $\mathbf{p} = (5, 0.32, 0.16)$, Fig. 3 shows the root mean squared error (RMSE) of the estimated distances, defined as $\sqrt{\mathbb{E}[\|\mathbf{d} - \hat{\mathbf{d}}\|^2]}$, versus the signal to noise ratio (SNR) of the received signal via the RUSs, which is defined as

$$\text{SNR} = \frac{\|S\tilde{\mathbf{w}}\|^2}{\|\eta\|^2} = \frac{P_t\|\tilde{\mathbf{w}}\|^2}{\sigma^2 K f_d}, \quad (55)$$

according to (25). It varies as a function of the total transmit power P_t . The distance estimated by the conventional method based on Time of Flight (ToF) is drawn from the Gaussian distribution $\mathcal{CN}(0, \sigma_{\text{ToF}}^2)$ where σ_{ToF}^2 is 1 ns [27]. For the estimated distance, it is observed that the RMSE under the proposed JMMSE method is much smaller than the other three schemes. The RMSEs under MMSE and MP are both smaller than the ToF scheme when the SNR is greater than -5 dB.

Combining the aforementioned distance estimation methods and the CML localization method, Fig. 4 shows the RMSE of

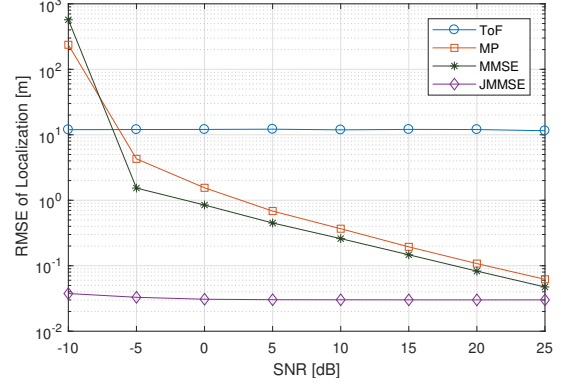


Fig. 4. The RMSE performance of the localization vs SNR of the received signal via the RUSs.

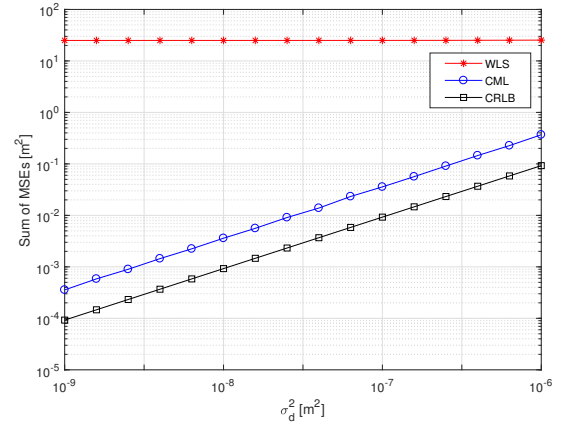


Fig. 5. The MSE performance of the 3D coplanar localization method versus the distance error σ_d^2 .

the localization of the UE, which is defined as $\sqrt{\mathbb{E}[\|\mathbf{p} - \hat{\mathbf{p}}\|^2]}$. Similar to the result of the distance estimation, the RMSE obtained by combining JMMSE and CML is much smaller than the other three schemes and achieves centimeter level positioning accuracy.

To analyze the performance of the proposed CML localization algorithm theoretically, we consider a fixed UE at $\mathbf{p} = (5, 0.32, 0.16)$, which is unknown to the system, and assume that all the estimated errors of the UE-RUS_m distances share the same noise variance σ_d^2 . That is, each error of the measured distance is drawn from $\mathcal{CN}(0, \sigma_d^2)$. The sum of the MSEs is defined as

$$\tilde{\mathcal{M}} = \mathcal{M}(x) + \mathcal{M}(y) + \mathcal{M}(z), \quad (56)$$

where $\mathcal{M}(x)$, $\mathcal{M}(y)$ and $\mathcal{M}(z)$ are the MSEs of the estimated x, y, z-coordinate of the UE respectively, e.g., $\mathcal{M}(x) = \mathbb{E}[(\hat{x} - \bar{x})^2]$. According to Theorem 2, the sum of CRLBs is defined as

$$\tilde{\mathcal{C}} = C_{11} + C_{22} + C_{33}. \quad (57)$$

Fig. 5 compares the sum of the MSE for the CML method with the corresponding CRLB and the traditional weighted least squares (WLS) algorithm [42]. The figure shows the proposed CML is much closer to the CRLB than the traditional WLS.

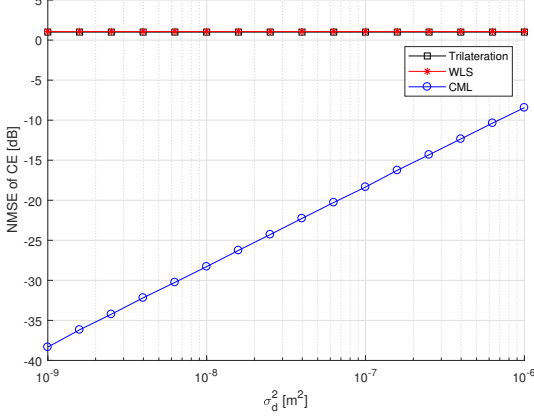


Fig. 6. The normalized MSE of the channel estimation versus the distance error σ_d^2 .

Further, we illustrate the performance of the proposed channel estimation scheme against the WLS algorithm and the conventional trilateration method [43]. The normalized MSE (NMSE) of the channel estimation is defined as

$$\text{NMSE} = \mathbb{E} \left[\frac{|w - \hat{w}|^2}{|w|^2} \right], \quad (58)$$

where w and \hat{w} denote the true cascaded BS-RIS-UE channel and the estimated channel, respectively. Fig. 6 shows the NMSE of channel estimation based on the aforementioned methods, and indicates that the proposed scheme can achieve lower NMSE than -15 dB when σ_d^2 is smaller than 10^{-7} , which outperforms the other two methods.

We consider a series of UE positions on the central perpendicular line (CPL) of the RIS and the total transmit power of the BS is fixed to $P_t = 30$ dBm. We combine the JMMSE distance estimation method and CML localization algorithm, which is labeled as ‘‘Proposed Method’’. The case calculated with the true position of the UE is marked as ‘‘Upper Bound’’, meaning that perfect CSI is known. In the ‘‘Uniform Random Case’’, the phase shift coefficient of each reflecting element on the RIS is a uniformly distributed random value which follows the distribution $\phi_n \sim \mathcal{U}(0, 2\pi)$. The performance of the JBF algorithm [20] is also shown as a baseline.

Fig. 7 shows the SNR of the received signal at the UE versus the x-coordinate of the UE. The proposed method has a higher SNR than the JBF algorithm, as it nearly achieves the upper bound and has around 40 dB gain over the random case.

Fig. 8 shows the throughput versus the x-coordinate of the UE. The throughput is defined as $\log_2(1+\text{SNR})$. It is observed that the throughput of the proposed method is much higher than the other three schemes and approaches the upper bound. Moreover, the proposed method provides around 13 bps/Hz higher throughput than the random case.

V. CONCLUSIONS

In this paper, we considered the channel estimation of an RIS-aided mmWave communication system. We first proposed the RUS concept for the purpose of positioning the UE based

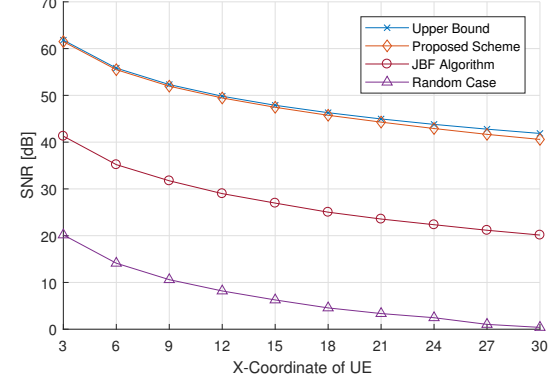


Fig. 7. The SNR of the received signal via the optimized RIS versus the X-coordinate of the UE.

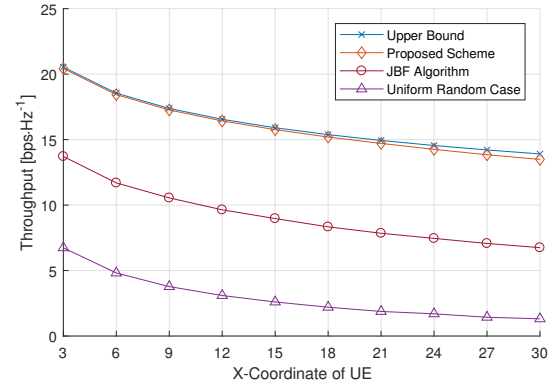


Fig. 8. The throughput at the receiver versus X-coordinate of the UE.

on the structure of the mmWave channel. We then proposed a CML 3D localization algorithm with a JMMSE distance estimation method. The CRLBs of the distance estimation error of our proposed method are derived. The CSI is reconstructed with the positioning results. Based on the sparse nature of the mmWave channel and the large size of the RIS, we showed the possibility of obtaining the channel information with very few training resources using our proposed method. Simulation results demonstrated significant performance gain in terms of the SNR of the received signal and the sum-rate.

APPENDIX A PROOF OF THEOREM 2

The distance between the UE and the m -th RUS is defined as:

$$d_m = \|\mathbf{p} - \mathbf{p}_m\| = [(\bar{x} - x_m)^2 + (\bar{y} - y_m)^2 + (\bar{z} - z_m)^2]^{\frac{1}{2}}, \quad (59)$$

the partial derivative of which with respect to $\mathbf{p}(i)$, $i = 1, 2, 3$, can be calculated as

$$\frac{\partial d_m}{\partial \mathbf{p}(i)} = \frac{\mathbf{p}(i) - \mathbf{p}_m(i)}{d_m} \quad (60)$$

The log-likelihood of (32) is

$$\ln P(\hat{\mathbf{d}}|\mathbf{p}) = - \sum_{m=1}^M \frac{(\hat{d}_m - d_m)^2}{2\sigma_d^2} - \sum_{m=1}^M \ln \sqrt{2\pi\sigma_d^2} \quad (61)$$

and the partial derivative of (61) with respect to $\mathbf{p}(i)$ is

$$\begin{aligned} \frac{\partial \ln P(\hat{\mathbf{d}}|\mathbf{p})}{\partial \mathbf{p}(i)} &= -\sum_{m=1}^M \frac{\partial}{\partial \mathbf{p}(i)} \left[\frac{(\hat{d}_m - d_m)^2}{2\sigma_d^2} \right] \\ &= \sum_{m=1}^M \frac{(\hat{d}_m - d_m)[\mathbf{p}(i) - \mathbf{p}_m(i)]}{\sigma_d^2 d_m} \end{aligned} \quad (62)$$

Further, the second partial derivative of (32) with respect to $\mathbf{p}(i)$ and $\mathbf{p}(j)$ is

$$\begin{aligned} \frac{\partial^2 \ln P(\hat{\mathbf{d}}|\mathbf{p})}{\partial \mathbf{p}(i) \partial \mathbf{p}(j)} &= \sum_{m=1}^M \frac{1}{\sigma_d^2} \frac{\partial}{\partial \mathbf{p}(j)} \left[\frac{(\hat{d}_m - d_m)[\mathbf{p}(i) - \mathbf{p}_m(i)]}{d_m} \right] \\ &= \sum_{m=1}^M \frac{1}{\sigma_d^2} \left[-\frac{[\mathbf{p}(i) - \mathbf{p}_m(i)] \cdot [\mathbf{p}(j) - \mathbf{p}_m(j)]}{d_m^2} \right. \\ &\quad \left. + \frac{(\hat{d}_m - d_m)[\mathbf{p}(i) - \mathbf{p}_m(i)] \cdot [\mathbf{p}(j) - \mathbf{p}_m(j)]}{d_m^3} \right] \end{aligned} \quad (63)$$

Since Δd_m follows a Gaussian distribution, $\mathbb{E}[\hat{d}_m - d_m] = 0$. The element of the FIM is expressed as:

$$\begin{aligned} \Psi_{ij} &= -\mathbb{E} \left[\frac{\partial^2 \ln P(\hat{\mathbf{d}}|\mathbf{p})}{\partial \mathbf{p}(i) \partial \mathbf{p}(j)} \right] \\ &= \sum_{m=1}^M \frac{1}{\sigma_d^2} \frac{[\mathbf{p}(i) - \mathbf{p}_m(i)] \cdot [\mathbf{p}(j) - \mathbf{p}_m(j)]}{d_m^2}, \end{aligned} \quad (64)$$

Finally, the CRLB matrix can be expressed as:

$$\mathbf{C} = \begin{bmatrix} C_{11} & C_{12} & C_{13} \\ C_{21} & C_{22} & C_{23} \\ C_{31} & C_{32} & C_{33} \end{bmatrix} = \Psi^{-1}. \quad (65)$$

REFERENCES

- [1] Y. Cui and H. Yin, "Channel estimation for RIS-aided mmWave communications via 3D positioning," in *Proc. IEEE/CIC Int. Conf. Commun. China (ICCC)*, Jul. 2021, pp. 399–404.
- [2] T. S. Rappaport, S. Sun, R. Mayzus, H. Zhao, Y. Azar, K. Wang, G. N. Wong, J. K. Schulz, M. Samimi, and F. Gutierrez, "Millimeter wave mobile communications for 5G cellular: It will work!" *IEEE Access*, vol. 1, pp. 335–349, 2013.
- [3] M. Di Renzo, K. Ntontin, J. Song, F. H. Danufane, X. Qian, F. Lazarakis, J. De Rosny, D.-T. Phan-Huy, O. Simeone, R. Zhang, M. Debbah, G. Lerohey, M. Fink, S. Tretyakov, and S. Shamai, "Reconfigurable intelligent surfaces vs. relaying: Differences, similarities, and performance comparison," *IEEE Open J. Commun. Soc.*, vol. 1, pp. 798–807, 2020.
- [4] M. Di Renzo, A. Zappone, M. Debbah, M.-S. Alouini, C. Yuen, J. de Rosny, and S. Tretyakov, "Smart radio environments empowered by reconfigurable intelligent surfaces: How it works, state of research, and the road ahead," *IEEE J. Sel. Areas Commun.*, vol. 38, no. 11, pp. 2450–2525, 2020.
- [5] M. Di Renzo, F. H. Danufane, and S. Tretyakov, "Communication models for reconfigurable intelligent surfaces: From surface electromagnetics to wireless networks optimization," *arXiv:2110.00833*, 2021. [Online]. Available: <https://arxiv.org/abs/2110.00833>
- [6] Q. Wu and R. Zhang, "Intelligent reflecting surface enhanced wireless network via joint active and passive beamforming," *IEEE Trans. Wireless Commun.*, pp. 1–1, Aug. 2019.
- [7] W. Tang, X. Li, J. Y. Dai, S. Jin, Y. Zeng, Q. Cheng, and T. J. Cui, "Wireless communications with programmable metasurface: Transceiver design and experimental results," *China Commun.*, vol. 16, no. 5, pp. 46–61, May. 2019.
- [8] W. Tang, M. Z. Chen, X. Chen, J. Y. Dai, Y. Han, M. Di Renzo, Y. Zeng, S. Jin, Q. Cheng, and T. J. Cui, "Wireless communications with reconfigurable intelligent surface: Path loss modeling and experimental measurement," *IEEE Trans. Wireless Commun.*, vol. 20, no. 1, pp. 421–439, 2021.
- [9] W. Tang, X. Chen, M. Z. Chen, J. Y. Dai, Y. Han, M. Di Renzo, S. Jin, Q. Cheng, and T. J. Cui, "Path loss modeling and measurements for reconfigurable intelligent surfaces in the millimeter-wave frequency band," *arXiv:2101.08607*, 2021. [Online]. Available: <https://arxiv.org/abs/2101.08607>
- [10] L. Dai, B. Wang, M. Wang, X. Yang, J. Tan, S. Bi, S. Xu, F. Yang, Z. Chen, M. Di Renzo, C. B. Chae, and L. Hanzo, "Reconfigurable intelligent surface-based wireless communications: Antenna design, prototyping, and experimental results," *IEEE Access*, vol. 8, pp. 45913–45923, 2020.
- [11] X. Pei, H. Yin, L. Tan, L. Cao, Z. Li, K. Wang, K. Zhang, and E. Björnson, "RIS-aided wireless communications: Prototyping, adaptive beamforming, and indoor/outdoor field trials," *IEEE Trans. Commun.*, vol. 69, no. 12, pp. 8627–8640, Dec. 2021.
- [12] T. Hou, Y. Liu, Z. Song, X. Sun, Y. Chen, and L. Hanzo, "Reconfigurable intelligent surface aided NOMA networks," *IEEE J. Select. Areas Commun.*, vol. 38, no. 11, pp. 2575–2588, Nov. 2020.
- [13] C. Pan, G. Zhou, K. Zhi, S. Hong, T. Wu, Y. Pan, H. Ren, M. Di Renzo, A. L. Swindlehurst, R. Zhang *et al.*, "An overview of signal processing techniques for ris/irs-aided wireless systems," *arXiv:2112.05989*, 2021. [Online]. Available: <https://arxiv.org/abs/2112.05989>
- [14] D. Mishra and H. Johansson, "Channel estimation and low-complexity beamforming design for passive intelligent surface assisted MISO wireless energy transfer," in *Proc. IEEE Int. Conf. Acoust., Speech Signal Process. (ICASSP)*, May 2019, pp. 4659–4663.
- [15] T. L. Jensen and E. D. Carvalho, "An optimal channel estimation scheme for intelligent reflecting surfaces based on a minimum variance unbiased estimator," in *Proc. IEEE Int. Conf. Acoust., Speech Signal Process. (ICASSP)*, May 2020, pp. 5000–5004.
- [16] Z. Wang, L. Liu, and S. Cui, "Channel estimation for intelligent reflecting surface assisted multiuser communications: Framework, algorithms, and analysis," *IEEE Trans. Wireless Commun.*, vol. 19, no. 10, pp. 6607–6620, Oct. 2020.
- [17] L. Wei, C. Huang, G. C. Alexandropoulos, C. Yuen, Z. Zhang, and M. Debbah, "Channel estimation for RIS-empowered multi-user MISO wireless communications," *IEEE Trans. Commun.*, pp. 1–1, 2021.
- [18] J. Chen, Y.-C. Liang, H. V. Cheng, and W. Yu, "Channel estimation for reconfigurable intelligent surface aided multi-user MIMO systems," *arXiv:1912.03619*, 2019. [Online]. Available: <https://arxiv.org/abs/1912.03619>
- [19] P. Wang, J. Fang, H. Duan, and H. Li, "Compressed channel estimation for intelligent reflecting surface-assisted millimeter wave systems," *IEEE Signal Process. Lett.*, vol. 27, pp. 905–909, 2020.
- [20] Z. He and X. Yuan, "Cascaded channel estimation for large intelligent metasurface assisted Massive MIMO," *IEEE Wirel. Commun. Lett.*, vol. 9, no. 2, pp. 210–214, 2020.
- [21] H. Liu, X. Yuan, and Y. J. A. Zhang, "Matrix-calibration-based cascaded channel estimation for reconfigurable intelligent surface assisted multiuser MIMO," *IEEE J. Sel. Areas Commun.*, pp. 1–1, 2020.
- [22] C. Hu, L. Dai, S. Han, and X. Wang, "Two-timescale channel estimation for reconfigurable intelligent surface aided wireless communications," *IEEE Trans. Commun.*, vol. 69, no. 11, pp. 7736–7747, 2021.
- [23] A. Abrardo, D. Dardari, and M. Di Renzo, "Intelligent reflecting surfaces: Sum-rate optimization based on statistical position information," *IEEE Trans. Commun.*, vol. 69, no. 10, pp. 7121–7136, 2021.
- [24] H. Wymeersch and B. Denis, "Beyond 5G wireless localization with reconfigurable intelligent surfaces," in *Proc. IEEE Int. Conf. Commun. (ICC)*, 2020, pp. 1–6.
- [25] T. Ma, Y. Xiao, X. Lei, W. Xiong, and Y. Ding, "Indoor localization with reconfigurable intelligent surface," *IEEE Commun. Lett.*, pp. 1–1, 2020.
- [26] J. He, H. Wymeersch, T. Sanguanpuak, O. Silven, and M. Juntti, "Adaptive beamforming design for mmWave RIS-aided joint localization and communication," in *Proc. IEEE Wireless Commun. Net. Conf. Work. (WCNCW)*, 2020, pp. 1–6.
- [27] F. Lemic, J. Martin, C. Yarp, D. Chan, V. Handziski, R. Brodersen, G. Fettweis, A. Wolisz, and J. Wawrzynek, "Localization as a feature of mmWave communication," in *Proc. Int. Wireless Commun. Mobile Compu. Conf. (IWCMC)*, 2016, pp. 1033–1038.
- [28] 3GPP, NR; *Physical Channels and Modulation (Release 15)*. Technical Specification TS 38.211, available: <http://www.3gpp.org>.
- [29] B. Di, H. Zhang, L. Li, L. Song, Y. Li, and Z. Han, "Practical hybrid beamforming with finite-resolution phase shifters for reconfigurable intelligent surface based multi-user communications," *IEEE Trans. Veh. Technol.*, vol. 69, no. 4, pp. 4565–4570, 2020.

- [30] E. Basar and I. Yildirim, "SimRIS channel simulator for reconfigurable intelligent surface-empowered communication systems," in *2020 IEEE Latin-American Conf. Commun. (LATINCOM)*, 2020, pp. 1–6.
- [31] M. F. Imani, D. R. Smith, and P. Hougne, "Perfect absorption in a disordered medium with programmable meta-atom inclusions," *Adv. Funct. Mater.*, vol. 30, no. 52, p. 2005310, Dec. 2020.
- [32] S. Li, F. Xu, X. Wan, T. J. Cui, and Y. Q. Jin, "Programmable meta-surface based on substrate-integrated waveguide for compact dynamic-pattern antenna," *IEEE Trans. Antennas Propag.*, pp. 1–1, 2020.
- [33] Z. Zhang, L. Dai, X. Chen, C. Liu, F. Yang, R. Schober, and H. V. Poor, "Active RIS vs. passive RIS: Which will prevail in 6G?" *arXiv:2103.15154*, 2021. [Online]. Available: <https://arxiv.org/abs/2103.15154>
- [34] 3GPP, 5G; NR; *Physical Layer Procedures for Data (Release 15)*. Technical Specification TS 38.214, available: <http://www.3gpp.org>.
- [35] Y. Hua and T. K. Sarkar, "Matrix pencil method for estimating parameters of exponentially damped/undamped sinusoids in noise," *IEEE Trans. Acoust., Speech, Signal Process.*, vol. 38, no. 5, pp. 814–824, 1990.
- [36] A. Gabel and A. Omar, "A study of wireless indoor positioning based on joint TDOA and DOA estimation using 2-D matrix pencil algorithms and IEEE 802.11ac," *IEEE Trans. Wireless Commun.*, vol. 14, no. 5, pp. 2440–2454, 2015.
- [37] E. H. Gismalla and E. Alsusa, "On the performance of energy detection using Bartlett's estimate for spectrum sensing in cognitive radio systems," *IEEE Trans. Signal Process.*, vol. 60, no. 7, pp. 3394–3404, Jul. 2012.
- [38] H. Yin, D. Gesbert, M. Filippou, and Y. Liu, "A coordinated approach to channel estimation in large-scale multiple-antenna systems," *IEEE J. Sel. Areas Commun.*, vol. 31, no. 2, pp. 264–273, Feb. 2013.
- [39] K. Cheung, H. So, W.-K. Ma, and Y. Chan, "Least squares algorithms for time-of-arrival-based mobile location," *IEEE Trans. Signal Process.*, vol. 52, no. 4, pp. 1121–1130, 2004.
- [40] Y. T. Chan and K. C. Ho, "A simple and efficient estimator for hyperbolic location," *IEEE Trans. Signal Process.*, vol. 42, no. 8, pp. 1905–1915, 1994.
- [41] Y.-T. Chan, H. Yau Chin Hang, and P. chung Ching, "Exact and approximate maximum likelihood localization algorithms," *Trans. Veh. Technol.*, vol. 55, no. 1, pp. 10–16, 2006.
- [42] D. Ni, O. A. Postolache, C. Mi, M. Zhong, and Y. Wang, "UWB indoor positioning application based on Kalman filter and 3-D TOA localization algorithm," in *Proc. Int. Symp. Adv. Topics Electr. Eng. (ATEE)*, 2019, pp. 1–6.
- [43] E. Doukhnitch, M. Salamah, and E. Ozen, "An efficient approach for trilateration in 3D positioning," *Computer Communications*, vol. 31, no. 17, pp. 4124–4129, 2008.